# Voxel-level Ventilation-Perfusion Functional Imaging for Lung RT: Proof-of-Concept Technical Feasibility and Preliminary Dosimetric Evaluation

**Suyan Bi[a], Wang X[a], Wan Sohaimi WF[ab*], Yusoff AL[ab*]**

[a]Department of Nuclear Medicine, Radiotherapy and Oncology, School of Medical Sciences, Health Campus, Universiti Sains Malaysia, Kelantan, Malaysia

[b]Hospital Pakar Universiti Sains Malaysia, Health Campus, Universiti Sains Malaysia, Kelantan, Malaysia

***Corresponding Author**: Dr. Ahmad Lutfi Yusoff
Department of Nuclear Medicine, Radiotherapy and Oncology, School of Medical Sciences, Health Campus, Universiti Sains Malaysia, Kelantan, Malaysia,
Email: alutfi@usm.my

## ABSTRACT

**INTRODUCTION:** Existing lung imaging lacks the dual assessment and spatial resolution needed for functional-avoidance radiotherapy. This proof-of-concept (PoC) feasibility study aimed to validate the technical feasibility of a novel voxel-level lung functional imaging technique based on ventilation-perfusion (VP) mapping and explore its preliminary utility in radiotherapy treatment planning. **MATERIALS AND METHODS:** We retrospectively analyzed 20 lung cancer patients with 4D-CT and PET/CT scans. Ventilation was calculated from 4D-CT deformable image registration, and perfusion from pre-processed PET images. High-function lung regions were defined as the top 40%. Three functional imaging modalities were generated: ventilation (V), perfusion (P), and VP imaging. The Dice Similarity Coefficient (DSC) and Bland-Altman plots evaluated agreement, and intensity-modulated radiation therapy (IMRT) plans were optimized for dosimetric comparison. **RESULTS:** The automated workflow took 45±15 minutes per patient, meeting clinical efficiency requirements. V-VP and P-VP showed moderate-to-good agreement in whole and low-function lungs (DSC up to 0.71; r up to 0.943) but poor agreement in high-function regions. VP-IMRT significantly reduced ipsilateral high-function lung V20Gy (81.03±56.03 to 61.14±64.44, $p<0.001$), with favourable dosimetric differences versus single-modality plans and no increased dose to organs at risk. **CONCLUSION:** VP-Imaging effectively integrates ventilation and perfusion data, establishes a reproducible workflow, and shows preliminary dosimetric advantages. This study prioritizes technical viability over diagnostic accuracy relative to SPECT V/Q, supporting the feasibility of VP-Imaging for personalized RT.

**KEYWORDS**: Voxel-grade; Ventilation-perfusion imaging; Radiotherapy; Deformable image registration.

## INTRODUCTION

Lung cancer accounts for over 1.8 million deaths annually worldwide, remaining the leading cause of cancer-related mortality.[1,2] For patients with inoperable or locally advanced non-small cell lung cancer (NSCLC), radiotherapy (RT) is a cornerstone of curative or palliative treatment. A major unmet challenge in thoracic RT is mitigating radiation-induced pulmonary injury (RIPI), which affects 10-30% of patients. It not only reduces quality of life but also limits RT dose escalation, compromising tumour control.[3,4] Functional lung imaging has emerged to identify regionally critical pulmonary parenchyma for functional avoidance RT, but existing modalities suffer from limitations that impede widespread clinical translation.

CT-based ventilation imaging (CTVI) integrates with RT workflows using 4D-CT data but captures only airflow, missing perfusion defects common in conditions where V/Q mismatch occurs.[5,6] PET-based perfusion imaging (PETPI) maps blood flow but cannot assess ventilation.[7,8] The gold-standard SPECT V/Q scans offer a combined assessment but suffer from low spatial resolution, require additional radiation, and increase patient burden.[9,10] Advanced MRI techniques are costly and inaccessible.[11] Compared with previous V/Q fusion approaches, the present study applies the Hadamard product between the normalized

Jacobian matrix from 4D-CT DIR and the normalized grayscale matrix from PET to achieve voxel-level ventilation-perfusion integration.[12,13] This strategy requires no extra dedicated imaging devices and can be directly incorporated into routine radiotherapy workflows.

This PoC feasibility study aims to de-risk technology development before larger trials,[14] deliberately omitting SPECT V/Q validation to prioritize workflow reproducibility. Our core objectives are: (1) establishing a reproducible pipeline for generating VP-Imaging from routine 4D-CT and PET/CT; (2) verifying coherent integration of ventilation and perfusion data; and (3) assessing preliminary dosimetric utility by testing if VP-guided RT plans reduce dose to high-function lung while maintaining tumour coverage.

## MATERIALS & METHODS

### Study Design and Scopes

This was a retrospective single-centre PoC feasibility study. It prioritized technical validation (workflow reproducibility, imaging agreement, preliminary dosimetric benefits) over clinical efficacy. The study flow is shown in Figure 1. Imaging data were retrieved from the TCIA dataset "CT-vs-pet-ventilation-imaging", including routine RT simulation scans of 20 lung cancer patients. Inclusion criteria required pathologically confirmed lung cancer, complete 4D-CT (10 phases) and PET/CT (18F-FDG), eligible image quality for DIR, and no prior thoracic RT/surgery.

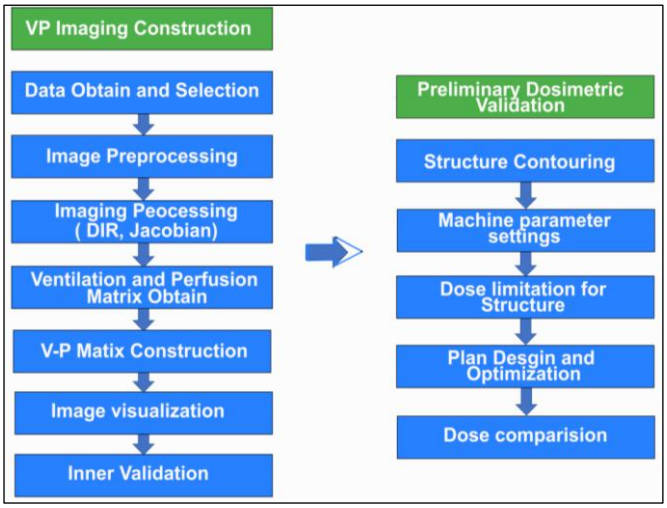


**Figure 1:** Study flow chart of this research

### Image Processing & Analysis Tools

Deformable image registration between inspiratory and expiratory 4D-CT phases was performed in 3D Slicer using a B-spline transformation.[15] The deformation vector field computed the Jacobian determinant for ventilation imaging. Subsequent analyses were implemented in Python with OpenCV, Scikit-Image, and NumPy for reproducibility.[16,17,18] F-FDG PET data were confined to lung mask voxels, smoothed, and normalized. VP maps were derived from the Hadamard product of normalized ventilation and perfusion matrices. Automated lung segmentation was validated against manual delineations by two radiation oncologists,[18] achieving a mean DSC of 0.92±0.03.

### Radiotherapy Treatment Planning

RT planning were conducted with VARIAN Eclipse™ using a 2.5 mm dose calculation grid.[19] All plans adopted identical optimization structures and dose-volume constraints, shown in Table I; hard dose limits were set for functional ROIs to achieve high-function lung avoidance, balanced with PTV coverage.

**Table I:** Dose targets and constraints for treatment planning

| Structure | Metrics | Objective |
|---|---|---|
| PTV | $V_{50Gy}$ | ≥95% |
| | $V_{55Gy}$ | <20% |
| | $D_{max}$ | <60 Gy |
| I-Lung | $V_{5Gy}$ | <60 % |
| | $V_{20Gy}$ | <20% |
| | $V_{30Gy}$ | <15% |
| | $D_{mean}$ | <15 Gy |
| I-Lung high40% | $D_{max}$ | <20 Gy |
| C-Lung | $V_{5Gy}$ | <20% |
| | $D_{mean}$ | <8 Gy |
| C-Lung high40% | $D_{max}$ | <20 Gy |
| I-40%HFV | $D_{10\%}$ | <5 Gy |
| | $D_{5\%}$ | <20 Gy |
| I-40%HFP | $D_{10\%}$ | <5 Gy |
| | $D_{5\%}$ | <20 Gy |
| I-40%HFVP | $D_{10\%}$ | <5 Gy |
| | $D_{5\%}$ | <20 Gy |
| C-40%HFV | $D_{max}$ | <5 Gy |
| C-40%HFP | $D_{max}$ | <5 Gy |
| C-40%HFVP | $D_{max}$ | <5 Gy |
| Heart | $D_{mean}$ | <4 Gy |
| | $V_{30Gy}$ | <40 % |
| | $V_{40Gy}$ | <30 % |
| Spinal cord | $D_{max}$ | <45 Gy |
| Oesophagus | $D_{max}$ | <52 Gy |

Noted: I=(Tumour) Ipsilateral; C=(Tumour) Contralateral; HF=High functional area; V=V-Imaging; P=P-Imaging; VP=VP-Imaging.

### Core Technical Pipeline & Metrics

Functional imaging utilized a sequential multi-modal pipeline:

i. V-Imaging: End-expiratory 4D-CT served as the reference; Jacobian determinants were used as a surrogate for local lung volume change[20,21] and classified into 11 functional levels, as illustrated in Figure 2.
ii. P-Imaging: Normalized PET values were divided into 11 functional levels via decile stratification.
iii. VP-Imaging Fusion: Normalized V/P matrices were fused by Hadamard products to generate VP-Imaging,[22] reclassified into 11 levels.

Feasibility was evaluated through workflow reproducibility (processing time and inter-operator DSC), imaging agreement (spatial overlap DSC and Bland-Altman consistency[23]), and dosimetric utility (dose reduction in four parallel IMRT plans: O-IMRT, V-IMRT, P-IMRT, VP-IMRT).[14] Statistical comparisons utilized repeated-measures ANOVA with Holm-Bonferroni correction.

## RESULTS

### Workflow Feasibility

The VP-Imaging pipeline, as shown in Figure 2, was successfully and reproducibly implemented in all 20 patients. The mean automated processing time was 45±15 minutes, well below the clinical target of ≤2 hours. The pipeline demonstrated excellent operator independence, yielding an inter-operator DSC of 0.89 for high-function lung regions.[24] Automated lung segmentations were highly consistent with manual delineations (DSC=0.92±0.03).[23]

### Imaging Agreement

VP-Imaging coherently integrated ventilation and perfusion data. Substantial spatial discordance occurred between standalone V-Imaging and P-Imaging (VP DSC=0.20±0.05), reflecting the complex pathophysiology of V/Q uncoupling in lung cancer. Integrated VP-Imaging showed significantly greater agreement with each modality map. For the whole lung, DSC values were 0.51±0.06 for V-VP and 0.54±0.12 for P-VP. Agreement peaked in low-function regions (bottom 30%), where P-VP reached a DSC of 0.71±0.09, as shown in Table II. All pairs exhibited low overlap (DSC≤0.35) in high-function regions, consistent with tumour-induced functional heterogeneity.[9]

**Table II:** DSC Values (Mean ± SD) for Imaging Pairs

| Region | V-P | V-VP | P-VP |
|---|---|---|---|
| Whole Lung | 0.20 ± 0.05 | 0.51 ± 0.06 | 0.54 ± 0.12 |
| Low-Function (Bottom 30%) | 0.21 ± 0.10 | 0.62 ± 0.08 | 0.71 ± 0.09 |
| High-Function (Top 40%) | 0.11 ± 0.03 | 0.34 ± 0.12 | 0.21 ± 0.04 |

VP-Imaging showed narrower 95% limits of agreement (LOA) and stronger correlations with single-modality imaging than the V-P pairing, see Figure 3. Correlation coefficients for the whole lung were 0.808 (V-P), 0.943 (V-VP), and 0.856 (P-VP). Cohort-level Bland-Altman analysis yielded a mean bias of 0.02, with a 95% LOA of -0.08 to 0.12 for VP-Imaging vs. V-Imaging, confirming that VP-Imaging provides substantially greater consistency than separate ventilation and perfusion maps without systematic bias.

### Preliminary Dosimetric Feasibility

All planning strategies (O-IMRT, V-IMRT, P-IMRT, VP-IMRT)[25] achieved clinically acceptable and statistically equivalent PTV coverage (V95%, $p>0.05$), with a typical dose distribution shown in Figure 4. VP-IMRT had a slightly higher mean PTV dose (52.46±0.63 Gy) than O-IMRT (51.90±0.80 Gy, $p=0.01$), representing a clinically insignificant difference of 1.12%. This confirms that VP-Imaging-guided planning preserves robust tumour coverage.[26,27] VP-IMRT achieved statistically significant dose reductions to the ipsilateral high-function lung compared with anatomical and single-modality plans, see Table III. The mean dose (Dmean) to the high-function lung was 8.00±5.06 Gy for VP-IMRT, significantly lower than 8.52±5.72 Gy for O-IMRT ($p<0.001$) and 8.61±4.29 Gy for P-IMRT ($p<0.001$). High-function lung volume receiving 20Gy (V20Gy) was heavily reduced to 61.14±64.44% in VP-IMRT, compared with 81.03 ± 56.03% in O-IMRT ($p<0.001$) and 137.54±82.74% in P-IMRT ($p<0.001$). Similar significant reductions were observed for V5Gy and V30Gy. These reductions align with core principles of functional avoidance radiotherapy,[2,28] and confirm VP-Imaging's potential to mitigate RIPI risk. Furthermore, no significant dose increases were observed for the heart, spinal cord, or esophagus in VP-IMRT compared with O-IMRT,

ensuring OAR safety. Similar significant reductions were observed for V5Gy and V30Gy in all functional plans versus O-IMRT (all $p<0.01$). No significant dose increases were observed for the heart, spinal cord, or esophagus in VP-IMRT compared with O-IMRT (Table III), confirming uncompromising OAR safety, important for clinical translation.[29,30]

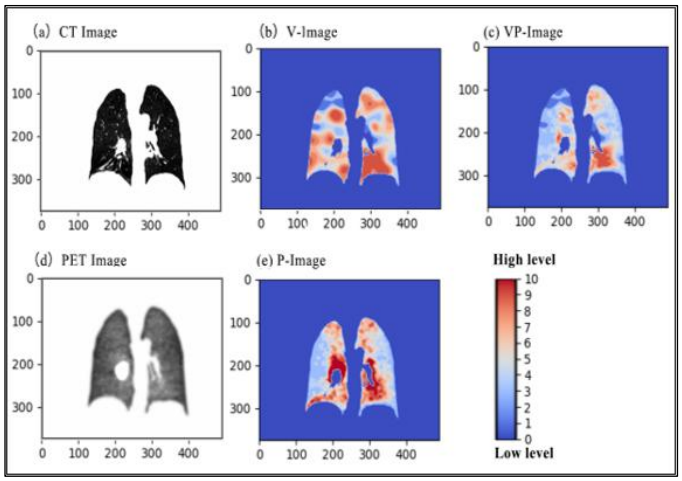


**Figure 2:** Representative VP-integrated functional imaging workflow for a locally advanced NSCLC patient undergoing radical RT (50 Gy/25 f): (a) Thoracic axial CT (anatomical baseline); (b) V-Imaging (DIR/Jacobian determinant); (c) P-Imaging (normalized $^{18}$F-FDG PET); (d) VP-Imaging (integrated V/P functional grading). A standardized colour map was applied: light grey = non-lung tissue (Grade 0), dark blue to bright red = ascending functional levels (Grade 1-10). Colour thresholds match Table I (octile, V-Imaging) and Table 2 (decile, P-/VP-Imaging), with all voxel-level grading within the automated lung segmentation mask (per Methods).

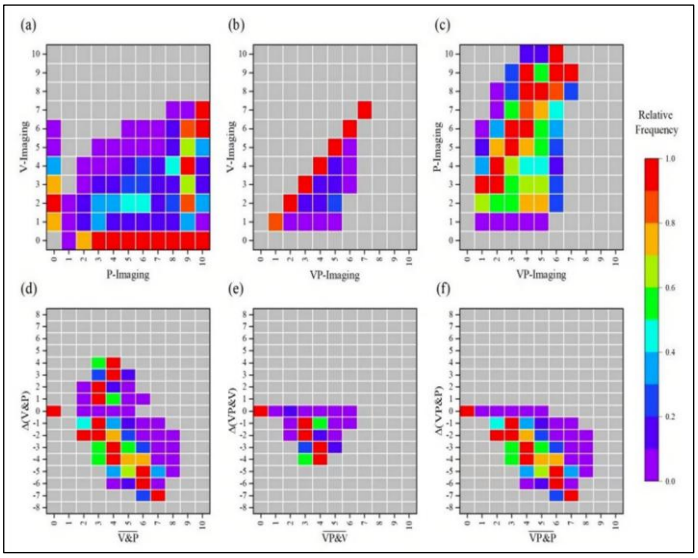


**Figure 3**: Cohort-level correlation and Bland-Altman analysis for whole-lung V-, P- and VP-Imaging in 20 locally advanced NSCLC patients. (a–c) V-P, V-VP, P-VP correlation scatter plots (Pearson coefficients: 0.808, 0.943, 0.856); (d-f) Bland-Altman plots (solid line= mean difference, dashed lines =95% LOA). A purple-to-bright red color map indicates low-to-high functional values (Grade 1-10, Tables 1-2; Grade 0 excluded). VP-Imaging vs. single-modality imaging had 95% LOA of ±0.08 to ±0.12, demonstrating good measurement consistency with no significant cohort-wide systematic bias.

Pairwise correlations among V-Imaging, P-Imaging, and VP-Imaging are shown in Fig. 3(a)-(c). Correlation coefficients for the whole lung were 0.808 (V-P), 0.943 (V-VP), and 0.856 (P-VP). Cohort-level Bland-Altman analysis (Figures 3(d)–(f)) yielded a mean bias of 0.02, with 95% LOA of -0.08 to 0.12 for VP-Imaging vs.

V-Imaging. For V-P, V-VP, and P-VP comparisons, the mean differences were 0.116, 0.071, and 0.045, with 95% CIs spanning ±1.241, ±0.699, and ±1.003, respectively. These intervals confirm that VP Imaging provides substantially greater consistency than separate ventilation and perfusion maps.

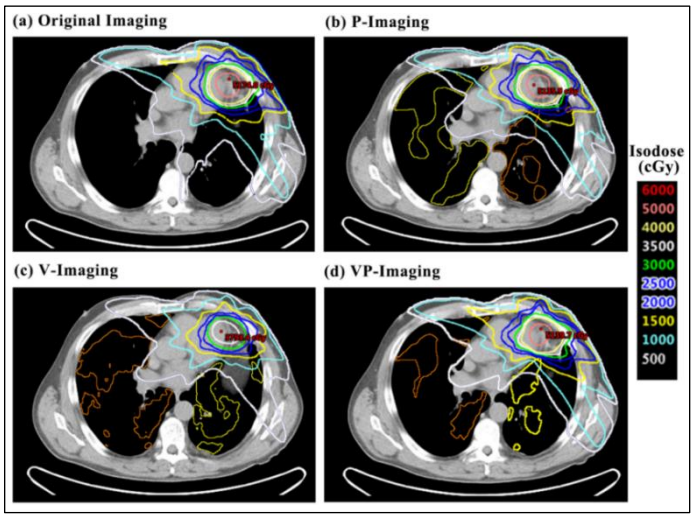


**Figure 4:** Representative axial dose distributions of O-IMRT and VP-IMRT for a patient with ipsilateral locally advanced NSCLC (radical 50 Gy/25 f):[31] (a) O-IMRT dose map; (b) VP-IMRT dose map with preferential sparing of high-function lung regions (bright red, Grade 10, Fig.4d). The 5 Gy (500 cGy) dose line (white contour) marks the key lung parenchyma low-dose threshold for radiation-induced pulmonary injury (RIPI) risk assessment, as V5Gy is the primary early endpoint for thoracic RT RIPI stratification. All doses are normalized to 50 Gy/25 f; the right color bar (0-60 Gy, linear scaling) shows dose intensity from low (white) to high (red).

**Table III:** Dose Parameters of Planning Target Volume (PTV) Across Four Radiotherapy Planning Strategies (x±s)

| PTV Dosimetric Index | O-IMRT | V-IMRT (Gy) | P-IMRT (Gy) | VP-IMRT | O vs V (p) | O vs P (p) | O vs VP (p) | F (RM-ANOVA) | RM-ANOVA p-value |
|---|---|---|---|---|---|---|---|---|---|
| $D_{max}$ (Gy) | 57.00±0.98 | 54.24±11.91 | 57.52±0.74 | 57.35±0.83 | 0.07 | 0.21 | 0.20 | 1.06 | 0.38 |
| $D_{5\%}$ (Gy) | 54.25±0.77 | 54.56±1.15 | 54.37±1.02 | 54.58±1.05 | 0.12 | 0.44 | 0.08 | 0.40 | 0.76 |
| $V_{95\%}$ (cc) | 58.50±38.14 | 58.42±38.08 | 58.45±38.15 | 54.93±40.69 | 0.09 | 0.27 | 0.31 | 0.03 | 0.99 |
| $D_{mean}$ (Gy) | 51.91±0.80 | 52.45±0.63 | 52.31±0.60 | 52.46±0.63 | <0.001 | 0.04 | 0.01 | 2.38 | 0.08 |
| $TV_{PTV}$ (cc) | 61.11±40.40 | 61.09±39.64 | 61.39±40.81 | 61.53±39.57 | 0.97 | 0.60 | 0.62 | 0.00 | 1.00 |
| TV (cc) | 58.62±38.35 | 58.62±38.35 | 58.62±38.35 | 58.62±38.35 | / | / | / | 0.00 | 1.00 |
| PIV (cc) | 55.69±36.43 | 55.69±36.43 | 55.69±36.43 | 55.69±36.43 | / | / | / | 0.00 | 1.00 |
| HI | 0.08±0.01 | 0.09±0.02 | 0.08±0.02 | 0.09±0.02 | 0.17 | 0.53 | 0.11 | 0.32 | 0.81 |
| CI | 1.18±0.13 | 1.17±0.11 | 1.18±0.13 | 1.20±0.11 | 0.59 | 0.82 | 0.32 | 0.21 | 0.89 |

Note: Abbreviations: Dmax = maximum dose; D5% = dose received by 5% of the PTV volume; V95% = percentage of PTV volume receiving ≥95% prescribed dose; Dmean = mean dose to PTV; TVPTV = target volume of PTV; TV = total tumor volume; PIV = planning internal volume; HI = Homogeneity Index; CI = Conformity Index. O-IMRT = anatomically guided IMRT; V-IMRT = ventilation-guided IMRT; P-IMRT = perfusion-guided IMRT; VP-IMRT = ventilation-perfusion integrated IMRT.

RM-ANOVA = repeated-measures analysis of variance (primary test for four within-patient planning strategies); post-hoc pairwise comparisons (O-IMRT vs V-/P-/VP-IMRT) were performed with Holm-Bonferroni correction for multiple testing; "/" = no statistical comparison (fixed anatomical indices with no inter-group variation); $p<0.05$ was considered statistically significant, and original "0.00" values were revised to <0.001 for statistical rigor.

Prescription dose: 50 Gy in 25 fractions (radical intent). A non-inferiority margin of ≤1–2% of the prescribed dose was used to define clinical insignificance for PTV dose differences.

**Table IV**: Dosimetric Parameters of Ipsilateral High-Function (HF) Lung Across Radiotherapy Planning Strategies (x±s)

| Dosimetric Index | O-IMRT (V-defined HF) | O-IMRT (P-defined HF) | O-IMRT (VP-defined HF) | V-IMRT | P-IMRT | VP-IMRT | P (V-IMRT vs. O-IMRT) | P (P-IMRT vs. O-IMRT) | P (VP-IMRT vs. O-IMRT) |
|---|---|---|---|---|---|---|---|---|---|
| $D_{mean}$ (Gy) | 7.00±4.19 | 9.31±4.50 | 8.52±5.72 | 6.64±4.12 | 8.61±4.29 | 8.00±5.06 | <0.001 | 0.03 | <0.001 |
| $V_{5Gy}$ (cc) | 171.67±112.92 | 281.35±134.21 | 150.97±160.23 | 164.60±113.02 | 269.02±126.60 | 148.42±158.23 | <0.001 | <0.001 | <0.001 |
| $V_{20Gy}$ (cc) | 81.03±56.03 | 151.45±92.64 | 69.48±71.02 | 72.20±52.88 | 137.54±82.74 | 61.14±64.44 | 0.01 | <0.001 | <0.001 |
| $V_{30Gy}$ (cc) | 42.08±32.88 | 86.42±57.43 | 35.13±34.59 | 39.85±31.64 | 81.91±54.26 | 33.38±32.15 | <0.001 | <0.001 | <0.001 |

Note: V/P/VP-defined HF： O-IMRT dosimetric data stratified by high-function lung regions defined by ventilation (V), perfusion (P), and ventilation-perfusion integrated (VP) imaging, respectively; O-IMRT = anatomically-guided IMRT; V-IMRT = ventilation-guided IMRT; P-IMRT = perfusion-guided IMRT; VP-IMRT = ventilation-perfusion integrated IMRT. Pairwise comparisons were performed using repeated-measures ANOVA with Holm-Bonferroni correction for multiple testing. Abbreviation： HF = High-Function; IMRT = Intensity-Modulated Radiotherapy.

## DISCUSSION

This PoC feasibility study validated a novel voxel-grade VP-Imaging technique for lung cancer RT, meeting three key feasibility endpoints: (1) Workflow feasibility via generation from routine 4D-CT/PET/CT without additional scans; (2) Imaging coherence demonstrating effective V/P integration via the Hadamard product; and (3) Dosimetric utility, as VP-IMRT reduced ipsilateral high-function lung Dmean and V20Gy versus standard planning while maintaining PTV coverage and OAR safety.

Adherence to PoC principles prioritized technical de-risking over immediate SPECT V/Q validation.[14] The pipeline's robust reproducibility justified deferring gold-standard comparisons, reinforcing VP-Imaging's distinct advantage of using routine staging scans to avoid extra patient radiation and cost. The open-source automated workflow achieved strong inter-operator consistency,[24] addressing the subjectivity of manual imaging[14,16] and enabling cross-institutional standardization. By applying Jacobian-based ventilation grading and the parameter-free Hadamard product,[24,32] this method outperformed alternative non-transparent fusion strategies. 3D deep learning may further optimize VP-Imaging.[33]

The dosimetric findings substantiate the clinical rationale for functional guidance. VP-IMRT successfully spared ipsilateral high-function lung parameters closely linked to radiation pneumonitis risk.[34] PTV coverage and doses to other organs at risk remained within clinical constraints across all plans.[26,27] Notably, VP-IMRT outperformed single-modality P-IMRT, as standalone P-Imaging is prone to overestimating function in tumour-adjacent V/Q mismatch areas.[9] Integrating ventilation and perfusion avoids this pitfall. Post hoc sensitivity analyses further confirmed that VP-Imaging classification is stable across moderate variations in DIR parameters and percentile binning thresholds, maintaining superior concordance compared to user-dependent weighted linear fusion models.

Inherent limitations exist, primarily the small retrospective cohort (n=20) and the absence of measured clinical endpoints. Future prospective trials are required to verify scalability, evaluate diagnostic accuracy against SPECT V/Q,[35,36] and track radiation pneumonitis incidence and post-RT lung function.

## CONCLUSION

This PoC feasibility study successfully validates the technical viability of a novel voxel-level VP-Imaging technique for lung cancer radiotherapy. A reproducible analytical pipeline is established using only routine

4D-CT and PET/CT scans. Ventilation and perfusion data are coherently integrated in the VP-Imaging modality, yielding favourable agreement with single-modality functional imaging. Preliminary dosimetric benefits are demonstrated via significant dose reductions to ipsilateral high-function lung tissue, achieved without compromising tumour target coverage or increasing radiation dose to organs at risk.

**FUNDING**

The research was funded by the Fundamental Research Grant Scheme (FRGS), year 2024, as mentioned in the acknowledgements.

**CONFLICT OF INTEREST**

There were no conflicts of interest between the contributors of this research.

**INSTITUTIONAL REVIEW BOARD (ETHICS COMMITTEE)**

This study was conducted in accordance with the Declaration of Helsinki and approved by the Ethics Committee of Universiti Sains Malaysia (USM/JEPeM/KK/24020139). The PyDICOM library was used to delete identifying tags, such as patient name and performing date-shifting for all dates by a fixed random number of days (±30 days) to ensure complete anonymization of patient information. Imaging data were obtained from The Cancer Imaging Archive (TCIA) public dataset "ct-vs-pet-ventilation-imaging" with collection URL: https://www.cancerimagingarchive.net/collection/ct-vs-pet-ventilation-imaging), accessed on [10/21, 2024], and all data usage strictly adhered to the TCIA Data Usage Policy. [37]

**ACKNOWLEDGEMENTS**

We would like to thank the Ministry of Higher Education for the research grant provided (FRGS/1/2024/SKK06/USM/02/5). We would also like to thank the Research Management Centre, USM, for facilitating the grant management (R503-KR-FRG001-0000000706-K134).

**REFERENCES**

1. Strange CD, Shroff GS, Truong MT, Net al. Imaging of the post-radiation chest in lung cancer. Clin Radiol. 2022;77(1):19-30. doi:10.1016/j.crad. 2021.04.013
2. Kimura T, Doi Y, Nakashima T, et al. Combined Ventilation and Perfusion Imaging Correlates With the Dosimetric Parameters of Radiation Pneumonitis in Radiation Therapy Planning for Lung Cancer. Int J Radiat Oncol Biol Phys. 2015;93(4):778-787. doi:10.1016/j.ijrobp.2015.08.024
3. Hanania AN, Mainwaring W, Ghebre YT, Hanania NA, Ludwig M. Radiation-Induced Lung Injury: Assessment and Management. Chest. 2019;156(1):150-162. doi:10.1016/j. chest.2019.03.033
4. Vinogradskiy Y, Castillo R, Castillo E, et al. Results of a Multi-Institutional Phase 2 Clinical Trial for 4DCT-Ventilation Functional Avoidance Thoracic Radiation Therapy. Int J Radiat Oncol Biol Phys. 2022;112(4):986-995. doi:10.1016/j.ijrobp.2021.10.147
5. Castillo E, Castillo R, Vinogradskiy Y, et al. Technical Note: On the spatial correlation between robust CT-ventilation methods and SPECT ventilation. Med Phys. 2020;47(11): 5731-5738. doi:10.1002/mp.14511
6. Vinogradskiy Y. CT-based ventilation imaging in radiation oncology. BJR Open. 2019;1(1):20180035. Published 2019 Apr 5. doi:10.1259/bjro 20180035

7. McIntosh L, Jackson P, Hardcastle N, et al. Automated assessment of functional lung imaging with 68Ga-ventilation/perfusion PET/CT using iterative histogram analysis. EJNMMI Phys. 2021;8(1):23. doi:10.1186/s40658-021-00375-6
8. Pinot F, Bourhis D, Bourbonne V, et al. New Automated Method for Lung Functional Volumes Delineation with Lung Perfusion PET/CT Imaging. Cancers (Basel). 2023;15(7):2166. doi:10.3390/cancers15072166
9. Lee SJ, Park HJ. Single photon emission computed tomography (SPECT) or positron emission tomography (PET) imaging for radiotherapy planning in patients with lung cancer: a meta-analysis. Sci Rep. 2020;10(1):14864. doi:10.1038/s41598-020-71445-5
10. Hoover DA, Reid RH, Wong E, et al. SPECT-based functional lung imaging for the prediction of radiation pneumonitis: a clinical and dosimetric correlation. J Med Imaging Radiat Oncol. 2014;58(2):214-222. doi:10.1111/1754-9485.12145
11. Ohno Y, Hanamatsu S, Obama Y, et al. Overview of MRI for pulmonary functional imaging. Br J Radiol. 2022;95(1132):20201053. doi:10.1259/bjr.20201053
12. K. Lee, H. Ko, D. Oh, J. Kim and H. Oh. Hadamard Product Arguments and Their Applications. in IEEE Access, 2025, 13: 79736-79756, 2025, doi: 10.1109/ ACCESS. 2025. 3566104.
13. G. Balakrishnan, A. Zhao, M. R. Sabuncu, J. Guttag and A. V. Dalca, "VoxelMorph: A Learning Framework for Deformable Medical Image Registration," in IEEE Transactions on Medical Imaging, 2019,38 (8): 1788-1800. doi: 10.1109/TMI.2019.2897538.
14. Kendig CE. What is Proof of Concept Research and how does it Generate Epistemic and Ethical Categories for Future Scientific Practice?. Sci Eng Ethics. 2016;22(3):735-753. doi:10.1007/s11948-015-9654-0
15. Castillo E, Castillo R, Vinogradskiy Y, et al. Robust CT ventilation from the integral formulation of the Jacobian. Med Phys. 2019;46(5):2115-2125. doi:10.1002/mp.13453
16. Rajasekar SJS, Thiyagarajan S, Mohamed Ali S. Ab.ai - A Novel Automated AI Tool for Reporting Antibiograms. Stud Health Technol Inform. 2022;299:202-207. doi:10.3233 /SHTI220984
17. Gouillart E, Nunez-Iglesias J, van der Walt S. Analyzing microtomography data with Python and the scikit-image library. Adv Struct Chem Imaging. 2017;2(1):18. doi:10.1186/ s40679-016-0031-0
18. Hofman MS, Beauregard JM, Barber TW, et al. 68Ga PET/CT ventilation-perfusion imaging for pulmonary embolism: a pilot study with comparison to conventional scintigraphy. J Nucl Med. 2011;52(10):1513-1519. doi:10.2967/jnumed.111.0 93344
19. Faghihi Moghaddam F, Bakhshandeh M, Ghorbani M, Mofid B. Assessing the out-of-field dose calculation accuracy by eclipse treatment planning system in sliding window IMRT of prostate cancer patients. Comput Biol Med. 2020;127:104052. doi:10.1016/ j.compbiomed.2020.104052
20. Zhong, W. J., Li, Y., & Cui, H. X. Application of 4D-CT-based lung functional imaging in radiotherapy for lung cancer[J]. Chinese Journal of Radiation Oncology, 2023, 44(8): 4045-4055. doi: 10.3760/cma.j.cn113030-20220414-00142
21. Xu, S., & Tian, L. DiffCNN: A collaborative framework of diffusion model and CNN for semi-supervised medical image segmentation. Neural Networks, 2025, 191, 107813. doi:10.1016/j.neunet.2025.107813
22. Honda N, Osada H, Watanabe W, et al. Imaging of ventilation with dual-energy CT during breath hold after single vital-capacity inspiration of stable xenon. Radiology. 2012;262(1):262-268. doi:10.1148/radiol.11110569

23. Bi S, Yuan Q, Dai Z, et al. Advances in CT-based lung function imaging for thoracic radiotherapy. Front Oncol. 2024;14:1414337. doi:10.3389/fonc.2024.1414337
24. Yeung M, Rundo L, Nan Y, Sala E, Schönlieb CB, Yang G. Calibrating the Dice Loss to Handle Neural Network Overconfidence for Biomedical Image Segmentation. J Digit Imaging. 2023;36(2):739-752. doi:10.1007/s10278-022-00735-3
25. Mounessi FS, Eckardt J, Holstein A, Ewig S, Könemann S. Image-based lung functional radiotherapy planning for non-small cell lung cancer. Strahlenther Onkol. 2020;196(2):151-158. doi:10.1007/s00066-019-01518-6
26. Fanetti G, Bazzani F, Ferrari A, et al. Bronchiolitis obliterans organizing pneumonia after stereotactic ablative radiation therapy for lung cancer: A case report. Cancer Radiother. 2018;22(1):57-61. doi:10.1016/j.canrad.2017.09.001
27. Espenel S, Chargari C, Blanchard P, et al. Practice changing data and emerging concepts from recent radiation therapy randomised clinical trials. Eur J Cancer. 2022;171:242-258. doi:10.1016/j.ejca.2022.04.038
28. Dougherty JM, Castillo E, Castillo R, et al. Functional avoidance-based intensity modulated proton therapy with 4DCT-derived ventilation imaging for lung cancer. J Appl Clin Med Phys. 2021;22(7):276-285. doi:10.1002/acm2.13323
29. Benveniste MF, Betancourt Cuellar SL, Gomez D, et al. Imaging of Radiation Treatment of Lung Cancer. Semin Ultrasound CT MR. 2018;39(3):297-307. doi:10.1053/j.sult.2018.02.002
30. Liu W, Feng H, Taylor PA, et al. NRG Oncology and Particle Therapy Co-Operative Group Patterns of Practice Survey and Consensus Recommendations on Pencil-Beam Scanning Proton Stereotactic Body Radiation Therapy and Hypofractionated Radiation Therapy for Thoracic Malignancies. Int J Radiat Oncol Biol Phys. 2024;119(4):1208-1221. doi:10.1016/j.ijrobp.2024.01.216
31. Kong, F. M., Ritter, T., Quint, D. J., et al. Consideration of dose limits for organs at risk of thoracic radiotherapy: atlas for lung, proximal bronchial tree, esophagus, spinal cord, ribs, and brachial plexus. International journal of radiation oncology, biology, physics, 2011, 81(5), 1442–1457. doi: 10.1016/j.ijrobp.2010.07.1977
32. Domínguez C, Heras J, Pascual V. IJ-OpenCV: Combining ImageJ and OpenCV for processing images in biomedicine. Comput Biol Med. 2017;84:189-194. doi:10.1016/j.com pbiomed.2017.03.027
33. Wilding-McBride D, Lim J, Byrne H, O'Brien R. CT ventilation images produced by a 3D neural network show improvement over the Jacobian and HU DIR-based methods to predict quantized lung function. Med Phys. 2025;52(2):889-898. doi:10.1002/mp.17532
34. Yamamoto T, Kabus S, Bal M, et al. Changes in Regional Ventilation During Treatment and Dosimetric Advantages of CT Ventilation Image Guided Radiation Therapy for Locally Advanced Lung Cancer. Int J Radiat Oncol Biol Phys. 2018;102(4):1366-1373. doi:10.1016/j.ijrobp.2018.04.063
35. Takemoto S, Shibamoto Y, Hashizume C, et al. Changes in pulmonary function and their correlation with dose-volume parameters in patients undergoing stereotactic body radiotherapy for lung cancer. J Radiat Res. 2021;62(2):338-345. doi:10.1093/jrr/rraa131
36. Nakamura H, Hirai T, Kurosawa H, et al. Current advances in pulmonary functional imaging. Respir Investig. 2024;62(1):49-65. doi:10.1016/j.resinv.2023.09.004
37. Eslick, E. M., Kipritidis, J., Gradinscak, D., et al. CT Ventilation as a functional imaging modality for lung cancer radiotherapy (CT-vs-PET-Ventilation-Imaging) (Version 1) [Data set]. The Cancer Imaging Archive. 2022.